Dynamics of an Elastic Seesaw Rotor

Norimichi Kawakami*
Fuji Heavy Industries LTD., Utsunomiya, Tochigi, Japan

A new method to analyze dynamic behavior of a seesaw rotor is presented. The derived equation of motion can be used to calculate the stability and performance of an elastic seesaw rotor by using Gessow's method which, prior to this study, has been limited to a nonelastic rotor. The equation of motion also includes the Blankenship method for calculation of the load distribution on a seesaw rotor in more refined form. Applying the classical representation of the airload, the equation of motion can be represented in analytical form thereby facilitating theoretical study. The "generalized Lock number" and the damping coefficient of each elastic mode are derived. The total number of modes necessary for convergence in the load calculation and the effect of elastic deformation on air load are also studied. It is demonstrated that the mode acceleration method is much more suitable for rotor load calculation than the usual mode displacement method.

Introduction

FOR the dynamic analysis of the articulated and the rigid rotor, it is usually sufficient to trace only the motion of one blade and to analyze its behavior. In the analysis of the seesaw rotor, however, it is necessary to treat two blades simultaneously because two blades are rigidly connected to each other and attached to the mast through a flapping hinge. Thus, when it is required to take account of blade elasticity, the treatment becomes much more difficult and complex.

Gessow[1] presented a method to study the motion of a seesaw rotor under extreme operating conditions in which nonlinearities such as stall, reversed flow, and the effect of compressibility are pronounced; but this method was restricted to the nonelastic rotor. Blankenship[2] developed a load calculation method for a seesaw rotor which, applying very intuitive techniques for the boundary conditions, made calculation possible by tracing the motion of one blade. It, however, has some difficulties accounting for the effect of blade elastic deformation on the airloading and is not suitable for studying the dynamics of an elastic rotor.

The emphasis of this paper is on deriving a fundamental equation of motion for a seesaw rotor that allows study of the dynamics of an elastic seesaw rotor. With the derived equation, performance calculation and load calculation can be performed with the same calculating effort as the articulated or the rigid rotor. Then, at the sacrifice of losing some precision, classical representation of airloads is substituted in the equation. It will be shown that a wide comprehension of the dynamics of an elastic seesaw rotor is possible by this analytical equation.

Derivation of the Equation of Motion

The equation describing the state of the equilibrium of forces acting on a beam that is rotating at a constant rpm about the shaft (see Fig. 1) is given by the following.[3]

$$\frac{\partial^2}{\partial r^2}\left(EI\frac{\partial^2 y}{\partial r^2}\right)-\Omega^2\frac{\partial}{\partial r}\left\{\left(\int_r^R m\eta\,d\eta\right)\frac{\partial y}{\partial r}\right\}=-m\Omega^2\frac{\partial^2 y}{\partial \psi^2}+f \tag{1}$$

where

$y=y(r,\psi)$ = vertical deflection of the beam
$EI=EI(r)$ = bending rigidity distribution
$m=m(r)$ = mass distribution
$f=f(r,\psi)$ = external loads distribution
R = radius of the beam
r = radial station
Ω = shaft angular velocity
ψ = azimuth angle

If the external loads distribution f should be zero, then Eq. (1) becomes the equation of the natural vibration of the same beam. At this time, the fact that there exist two kinds of modal series in a seesaw rotor must be noted. Namely, the blades can vibrate both antisymmetrically and symmetrically. The former is named cyclic mode, and the latter is collective (see Fig. 2). These modal series are calculated with the following root boundary conditions.

(A) Cyclic mode displacement = moment = 0

(B) Collective mode displacement = slope = 0

Condition (A) is the same for an articulated rotor with zero offset hinges and condition (B) is the same for a rigid rotor. Thus, represent each modal series as

$$(\omega_n^A,\ \phi_n^A)\quad(\omega_n^R,\ \phi_n^R)\qquad(n=1,2,3)\tag{2}$$

where ω_n is the nth natural frequency, ϕ_n represents the nth natural vibration mode, and superscript A is articulated and R is rigid. It is well known that the natural vibration modes possess the following conditions of orthogonality

$$\int_0^R m\phi_i^A\phi_j^A\,dr=\int_0^R m\,\phi_i^R\phi_j^R\,dr=0\qquad(i\neq j)\tag{3}$$

When i is equal to j, the integrations have nonzero values, but the absolute values can be defined somewhat freely cor-

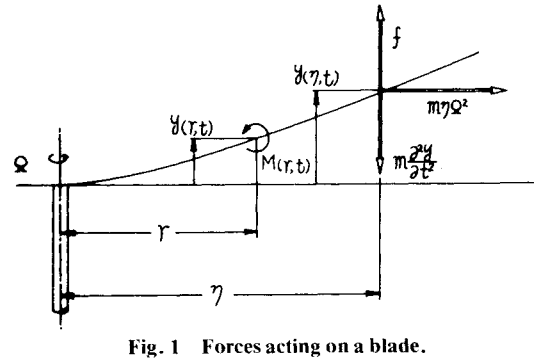

Fig. 1 Forces acting on a blade.

Received May 14, 1975; revision received Sept. 20, 1976.
Index categories: Rotary Wing Aerodynamics; Aeroelasticity and Hydroelasticity; Structural Dynamic Analysis.

*Helicopter engineer, Helicopter and VTOL Section, Aircraft Engineering Division.

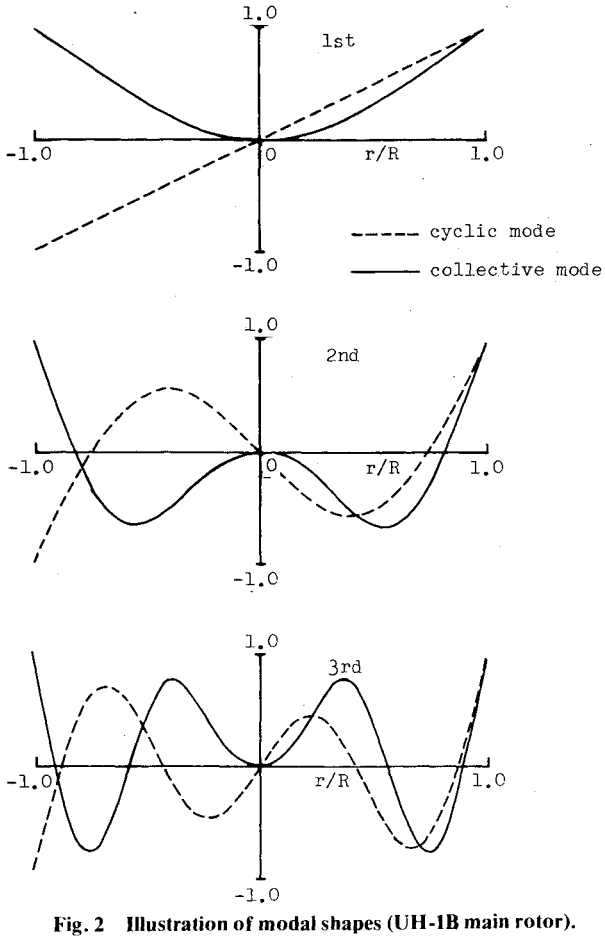

Fig. 2 Illustration of modal shapes (UH-1B main rotor).

responding to the normalizing technique of ϕ. In this report, the following definitions are used

$$\phi_n^A(R)=\phi_n^R(R)=1 \tag{4}$$

$$\int_0^1 \bar{m}\phi_n^{A^2}\,dx=\frac{1}{Rm_0}\int_0^R m\phi_n^{A^2}\,dr\equiv M_n^A \tag{5}$$

$$\int_0^1 \bar{m}\phi_n^{R^2}\,dx=\frac{1}{Rm_0}\int_0^R m\phi_n^{R^2}\,dr\equiv M_n^R \tag{6}$$

In Eqs. (5) and (6), r and m are transformed to the non-dimensional values x and $\bar{m}$ by using the definition of

$$x=r/R \qquad \bar{m}=m/m_0 \quad (m_0\text{: reference mass})$$

Now represent the deformation function y which appears in Eq. (1) by using the modal function ϕ_n as follows

$$y(r,\psi)=R\sum_{n=1}^{\infty}\left\{q_n^A(\psi)\phi_n^A(r)+q_n^R(\psi)\phi_n^R(r)\right\}+a_0 r \tag{7}$$

wherein a_0 means the preconing angle. Substitution of Eq. (7) into Eq. (1) yields

$$R\sum_n(\Omega^2\ddot{q}_n^A+\omega_n^{A^2}q_n^A)m\phi_n^A$$

$$+R\sum_n(\Omega^2\ddot{q}_n^R+\omega_n^{R^2}q_n^R)m\phi_n^R=f-mr\,\Omega^2a_0 \tag{8}$$

where

$$\ddot{q}_n=d^2q_n/d\psi^2$$

Multiplying Eq. (8) by ϕ_n^A and integrating the product from the root to the tip together with the conditions (3) and (5) yields

$$Rm_0M_n^A(\Omega^2\ddot{q}_n^A+\omega_n^{A^2}q_n^A)+Rm_0\sum_k(\Omega^2\ddot{q}_k^R+\omega_k^{R^2}q_k^R)$$

$$\times\int_0^1\bar{m}\phi_k^R\phi_n^A\,dx=\int_0^1 f(x,\psi)\,\phi_n^A\,dx-m_0R\Omega^2a_0\int_0^1\bar{m}x\phi_n^A\,dx \tag{9}$$

Similarly, if Eq. (8) is multiplied by ϕ_n^R and integrated, the following equation results

$$Rm_0\sum_k(\Omega^2\ddot{q}_k^A+\omega_k^{A^2}q_n^A)\int_0^1\bar{m}\phi_k^A\phi_n^R\,dx$$

$$+Rm_0M_n^R(\Omega^2\ddot{q}_n^R+\omega_n^{R^2}q_n^R)$$

$$=\int_0^1 f(x,\psi)\phi_n^R\,dx-m_0R\Omega^2a_0\int_0^1\bar{m}x\phi_n^R\,dx \tag{10}$$

At this time, consider the other blade that leads by 180° azimuth angle to the azimuth angle of Eqs. (9) and (10). Since a seesaw rotor is being considered, the following relations must be realized

$$q_n^A(\psi+\pi)=-q_n^A(\psi) \qquad q_n^R(\psi+\pi)=q_n^R(\psi) \tag{11}$$

Thus, it is necessary to solve Eqs. (9) and (10) under the condition of Eq. (11) for the determination of the dynamic behavior of a seesaw rotor. It is, however, apparent that the calculation will become very complex because of the coupling between the two modal series. Furthermore, it is very formidable to solve the differential equations (9) and (10) satisfying the continuity condition of Eq. (11). To avoid these difficulties, a new theoretical technique has been devised as follows: By using the condition of Eq. (11), the following equations can be written for the other blade.

$$-Rm_0M_n^A(\Omega^2\ddot{q}_n^A+\omega_n^{A^2}q_n^A)$$

$$+RM_0\sum_k(\Omega^2\ddot{q}_k^R+\omega_k^{R^2}q_k^R)\int_0^1\bar{m}\phi_k^R\phi_n^A\,dx$$

$$=\int_0^1 f(x,\psi+\pi)\,\phi_n^A\,dx-m_0R\Omega^2a_0\int_0^1\bar{m}x\phi_n^q\,dx \tag{9'}$$

$$-Rm_0\sum_k(\Omega^2\ddot{q}_k^A+\omega_k^{A^2}q_k^A)\int_0^1\bar{m}\phi_k^A\phi_n^R\,dx$$

$$+Rm_0M_n^R(\Omega^2\ddot{q}_n^{R^2}+\omega_n^{R^2}q_n^R)$$

$$=\int_0^1 f(x,\psi+\pi)\phi_n^R\,dx-m_0R\Omega^2a_0\int_0^1\bar{m}x\phi_n^R\,dx \tag{10'}$$

Subtracting Eq. (9') from Eq. (9) yields

$$2Rm_0M_n^A(\Omega^2\ddot{q}_n^A+\omega_n^{A^2}q_n^A)=\int_0^1\{f(x,\psi)-f(x,\psi+\pi)\}\phi_n^A\,dx \tag{12}$$

Adding Eq. (10') to Eq. (10) yields

$$2Rm_0M_n^R(\Omega^2\ddot{q}_n^R+\omega_n^{R^2}q_n^R)=\int_0^1\{f(x,\psi)+f(x,\psi+\pi)\}\phi_n^R$$

$$-2m_0R\Omega^2a_0\int_0^1\bar{m}x\phi_n^R\,dx \tag{1}$$

These equations can be rewritten in more refined form as follows.

$$\ddot{q}_n^A + p_n^{A^2} q_n^A = \Xi_n^A \qquad \ddot{q}_n^R + p_n^{R^2} q_n^R = \Xi_n^R \quad (n=1,2,3\ \ldots) \tag{14}$$

where

$$\Xi_n^A = (1/2m_0R\Omega^2 M_n^A)\int_0^l \{f(x,\psi) - f(x,\psi+\pi)\}\phi_n^A \mathrm{d}x \tag{15}$$

$$\Xi_n^R = (1/2m_0R\Omega^2 M_n^R)\int_0^l \{f(x,\psi) + f(x,\psi+\pi)\}\phi_n^R \mathrm{d}x - (a_0/M_n^R)\int_0^l \bar{m}x\phi_n^R \mathrm{d}x \tag{16}$$

$$p_n^A = \omega_n^A/\Omega \qquad p_n^R = \omega_n^R/\Omega \tag{17}$$

It is apparent that Eq. (14) is no longer coupled elastically or inertially, and at the same time the subsidiary condition of Eq. (11) has already been included. Equation (14) is the fundamental equation of motion for the elastic seesaw rotor.

Relation to Previous Work

Let us, then, consider relations between the present results and the previous work. Two kinds of considerations will be taken: first, about the method of rotor performance and flapping analysis; and second, about the rotor load analysis.

Usually the analysis of the performance and the stability of the dynamic behavior of a seesaw rotor has been performed under an assumption that the rotor does not deform elastically. This assumption may be considered from the view point of present elastic rotor analysis in which account is taken of only the fundamental cyclic mode, ϕ_1^A, and all other modes are neglected. The fundamental cyclic mode is the rigid rotation around the hinge so that

$$\phi_1^A(x) = x \tag{18}$$

$$\omega_1^A = \Omega \qquad (p_1^A = 1) \tag{19}$$

Consequently, Eq. (7) becomes

$$y(r,\psi) = Rq_1^A(\psi)x + a_0 r = r\{q_1^A(\psi) + a_0\} \tag{20}$$

This equation means that the generalized coordinate q_1^A represents the inclination of the tip path plane and is related to the usual flap angle as follows

$$\beta(\psi) = q_1^A(\psi) + a_0 \tag{21}$$

By writing

$$2m_0R^3M_1^A = 2\int_0^R mr^2\mathrm{d}r = I \tag{22}$$

where $2m_0R^3M_1^A$ denotes the moment of inertia I of a seesaw rotor around the flapping hinge, the generalized force Ξ_1^A reduces to

$$\Xi_1^A = (1/I\,\Omega^2)\int_0^R \{f(r,\psi) - f(r,\psi+\pi)\}r\mathrm{d}r = M/I\,\Omega^2 \tag{23}$$

In Eq. (23), M is the external moment around the flapping hinge. Thus Eq. (14) becomes the following well-known equation which states the moment equilibrium condition for a seesaw rotor

$$\ddot{\beta} + \beta = M/I\,\Omega^2 + a_0 \tag{24}$$

Gessow presented a method to solve Eq. (24) by using the Runge-Kutta method together with numerical integration of Eq. (23). Thus his method makes it possible to analyze the performance and the dynamic behavior of a seesaw rotor under the extreme operating conditions in which nonlinearities such as stall, reversed flow, and the compressibility effect are pronounced. Although Gessow's method is restricted to only a nonelastic rotor, it is apparent that same analysis can be taken for the more realistic rotor if derived Eqs. (14)-(16) are used.

Blankenship developed a method to calculate load distribution on a seesaw rotor. In this method, the rotor is initially assumed rigid, and rotor motion is calculated by using Gessow's method. The resultant airload is decomposed into the Fourier series; then the forced sinusoidal motion of the elastic rotor blade can be calculated under the assumption that the root condition is simple support for Fourier odd terms and cantilever support for Fourier even terms. The moment and shear-force distributions are obtained by simple superposition of each sinusoidal value. By this intuitive method, the load calculation of a seesaw rotor, as well as a rigid or an articulated rotor, has been possible by tracing the motion of one blade. Some problems, however, remain as follows: First, it is difficult to calculate the effect of the elastic deformation on the airloading. Blankenship overcame this difficulty by the iteration method, but it seems that if any natural frequency of the rotor is near one of the Fourier frequencies there may be resonances. Second, for the sake of Fourier decomposition, any motion except stationary periodic motion can not be straightforwardly analyzed by this method. This becomes an obstacle in meneuver load calculation. Third, the analysis of the rotor flapping motion and the load analysis are disconnected for each other, so that a comprehension of the dynamics of an elastic seesaw rotor is difficult. It is impossible to know the effect of, for example, a small change of preconing angle on the moment distribution unless a numerical analysis is performed.

It is apparent that Eqs. (14)-(16) are closely related to the Blankernship method. Namely, the calculation $f(x,\psi) - f(x,\psi+\pi)$ in Eq. (15) nullifies the Fourier even terms. Thus, there are only Fourier odd terms in the generalized force that determine the magnitude of the antisymmetric modes (satisfying the simple support root condition). Similary, Ξ_n^R retains only the Fourier even terms and excites the symmetrical mode q_n^R that satisfies the cantilever root condition. It is evident that the problems experienced in the Blankenship method will almost disappear if Eqs. (14)-(16) are used.

It may be concluded from the above considerations that the present method is an extension of the Gessow method to the elastic seesaw rotor and, at the same time, includes the Blankenship method in a more refined manner.

Some Considerations about the Rotor Load Calculation

If Eq. (14) is solved, the motion of an elastic seesaw rotor is determined completely. Consequently, the load analysis becomes a relatively easy task. There, however, remains one problem that needs to be examined, that is the rate of convergence in the load calculation. Namely, how many elastic modes should be retained?

Referring to Fig. 1, the bending moment and the shearing force acting at the radial station r are calculated by the following equations

$$M(r,\psi) = \int_r^R [\{f(\eta,\psi) - m\Omega^2\ddot{y}(\eta,\psi)\}(\eta - r) - m\eta\Omega^2\{y(\eta,\psi) - y(r,\psi)\}]\mathrm{d}\eta \tag{25}$$

$$S(r,\psi) = \int_r^R \{f(\eta,\psi) - m\Omega^2\ddot{y}(\eta,\psi)\}\mathrm{d}\eta \tag{26}$$

Using Eqs. (1) and (7), Eqs. (25) and (26) can be reduced to the following

$$M(r,\psi) = \sum_n \{q_n^A(\psi)\bar{M}_n^A(r) + q_n^R(\psi)\bar{M}_n^R(r)\} \tag{27}$$

$$S(r,\psi)=\sum_n \{q_n^A(\psi)\bar{S}_n^A(r)+q_n^R(\psi)\,\bar{S}_n^R(r)\} \tag{28}$$

where

$$\bar{M}_n^i=m_0R^3\Omega^2\{(\omega_n^{i2}-\Omega^2)\int_x^1 \bar{m}\eta\phi_n^i\mathrm{d}\eta$$
$$-\omega_n^{i2}x\int_x^1 \bar{m}\phi_n^i\mathrm{d}\eta+\Omega^2\phi_n^i\int_x^1 \bar{m}\eta\mathrm{d}\eta\} \tag{29}$$

$$\bar{S}_n^i=m_0R^2\Omega_n^{i2}\int_x^1 \bar{m}\phi_n^i\mathrm{d}\eta \qquad (i=A \text{ or } R) \tag{30}$$

and where $\bar{M}_n^A$, $\bar{M}_n^R$ represent the moment distribution of the nth natural vibration and, similarly, $\bar{S}_n^A$, $\bar{S}_n^R$ are the shear loadings. If the physical characteristics of the blade are known, these distribution functions can be calculated. Once these functions are determined, rotor loads can be calculated by a simple multiplication expressed by Eqs. (27) and (28). This calculating method is widely used in the rotor load analysis and is known as the mode displacement method (MDM).[3]

Shupe[4] expressed some question about the convergence rate in Eqs. (27) and (28) when studying the dynamics of a rigid rotor. Previously, Bramwell[5] used only one fundamental mode in the calculation of the control derivatives of a rigid rotor. Higher modes were neglected because the deflection of a rigid rotor can be expressed accurately using only one fundamental mode. This simplified calculating method is equivalent to the assumption that the rates of convergence both of the deflection equation (7) and of the load equations (27) and (28) are equal. However, as a matter of fact, these convergence rates are different. The generalized coordinates q_n usually diminish rapidly as n becomes large; consequently, the deflection curve can be represented with a relatively small number of mode shapes. The moment equation, however, does not converge so rapidly as the deflection because the curvature of the mode shape becomes greater with the higher mode.

It is desired from the calculation standpoint that as few as possible mode numbers should be retained in the equations. Referring to Shupe's suggestion, the equations for load calculation should be represented as follows: substituting Eq. (7) into Eq. (25) yields

$$M(x,\psi)=R^2\int_x^1 f(\eta,\psi)\,(\eta-x)\mathrm{d}\eta$$
$$-m_0R^3\Omega^2\Big[\sum_n\Big\{\ddot{q}_n^A\int_x^1 \bar{m}\phi_n^A(\eta-x)\mathrm{d}\eta$$
$$+\ddot{q}_n^R\int_x^1 \bar{m}\phi_n^R(\eta-x)\mathrm{d}\eta\Big\}+\sum_n\Big\{q_n^A\Big(\int_x^1 \bar{m}\eta\phi_n^A\mathrm{d}\eta-\phi_n^A\int_x^1 \bar{m}\eta\mathrm{d}\eta\Big)$$
$$+q_n^R\Big(\int_x^1 \bar{m}\eta\phi_n^R\mathrm{d}\eta-\phi_n^R\int_x^1 \bar{m}\eta\mathrm{d}\eta\Big)\Big\}+a_0\Big\{\int_x^1 \bar{m}\eta^2\mathrm{d}\eta-x\int_x^1 \bar{m}\eta\mathrm{d}\eta\Big\}\Big] \tag{31}$$

Now, make the following definitions

$$\lambda_n^i(x)=\int_x^1 \bar{m}\eta\phi_n^i\mathrm{d}\eta \qquad \sigma_n^i(x)=\int_x^1 \bar{m}\phi_n^i\mathrm{d}\eta$$
$$\tau(x)=\int_x^1 \bar{m}\eta\mathrm{d}\eta \qquad k(x)=\int_x^1 \bar{m}\eta^2\mathrm{d}\eta \qquad (i=A \text{ or } R) \tag{32}$$

All terms except $\ddot{q}_n^A$ and $\ddot{q}_n^R$ in Eq. (31) represent the moment distribution attained when the rotor deforms quasistatically. Thus Eq. (31) can be rewritten as follows.

$$M(x,\psi)=M_{\text{Static}}(x,\psi)+M_{\text{Dynamic}}(x,\psi) \tag{33}$$

$$M_{\text{Static}}=R^2\int_x^1 f\cdot(\eta-x)\mathrm{d}\eta-m_0R^3\Omega^2\Big[\sum_n\Big\{q_n^A(\lambda_n^A-\phi_n^A\tau)$$
$$+q_n^R(\lambda_n^R-\phi_n^R\tau)\Big\}+a_0\,(k-x\tau)\Big] \tag{34}$$

$$M_{\text{Dynamic}}=-m_0R^3\Omega^2\sum_n\{\ddot{q}_n^A(\lambda_n^A-x\sigma_n^A)+(q_n^R-x\sigma_n^R)\} \tag{35}$$

Similarly, the shear force distribution is expressed by

$$S(x,\psi)=S_{\text{Static}}(x,\psi)+S_{\text{Dynamic}}(x,\psi) \tag{36}$$

$$S_{\text{Static}}=R\int_x^1 f\mathrm{d}\eta \tag{37}$$

$$S_{\text{Dynamic}}=-m_0R^2\Omega^2\sum_n(\ddot{q}_n^A\sigma_n^A+\ddot{q}_n^R\sigma_n^R) \tag{38}$$

Equations (33) and (36) are known as the mode acceleration method (MAM) because of the acceleration terms $\ddot{q}_n$. The MAM converges much more rapidly than the MDM so that sometimes MAM has been used in the fixed wing field.[3] In the field of the rotor load analysis, it has been traditional to use the MDM; but, as will be shown in a numerical example, the same situation may be expected, and the MAM should be used.

Simplified Analytical Representation of the Equation of Motion

Nonlinearity effects can be taken into account using Eqs. (15) and (16) with the numerical integration method.

Calculations with nonlinear effects will be required in the detail design stage of a seesaw rotor. However, a more simplified analytic equation is also required to understand quickly the effects of any parameters that affect rotor dynamics. Thus, a more analytic representation of the seesaw rotor's equation of motion will be derived using the classical representation of the airload.

The external force f is composed of the airload and the gravity force if stationary level flight is assumed. Then, make some simplifications as follows:

a) neglect the stall effect
b) neglect the reversed flow effect
c) neglect the air compressibility
d) assume uniform downwash velocity field.

Integration of Eqs. (15) and (16) using the obvious assumptions gives the analytical representation of the generalized forces Ξ_n^A and Ξ_n^R. Then, Eq. (14) yields the following analytic equations of motion for a seesaw rotor.

$$\ddot{q}_n^A+p_n^{A2}q_n^A=\frac{1}{2}\gamma_n^A\Big[-\sum_m \dot{q}_m^A\,J_{1nm}^A$$
$$+\Big\{-\frac{1}{4}A_1\mu^2C_{0n}^A-A_1C_{2n}^A-\mu\sum_m q_m^R\,K_{1nm}^{AR}$$
$$-\mu a_0C_{1n}^A\Big\}\cos\psi+\Big\{\Big(\lambda\mu-\frac{3}{4}\mu^2B_1\Big)C_{0n}^A$$
$$-\mu\sum_m \dot{q}_m^R\,J_{0nm}^{AR}+2\mu\theta_0C_{1n}^A$$
$$+(2\mu\theta_1-B_1)C_{2n}^A\Big\}\sin\psi+\Big\{-\frac{1}{2}\mu^2\sum_m q_m^RK_{0nm}^{AR}\Big\}\sin 2\psi$$
$$+\Big\{\frac{1}{4}\mu^2A_1C_{0n}^A\Big\}\cos 3\psi+\Big\{\frac{1}{4}\mu^2B_1C_{0n}^A\Big\}\sin 3\psi\Big] \tag{39}$$

$$\ddot{q}_n^R + p_n^{R^2} q_n^R = \frac{1}{2}\gamma_n^R \Big[-\sum_m \dot{q}_m^R J_{1nm}^R + \frac{1}{2}\theta_0 \mu^2 C_{0n}^R + \Big(\frac{1}{2}\theta_1 \mu^2 - \mu B_1 + \lambda\Big) C_{1n}^R + \theta_0 C_{2n}^R + \theta_1 C_{3n}^R + \Big\{-\mu \sum_m q_m^A K_{1nm}^{RA}\Big\} \cos\psi + \Big\{-\mu \sum_m \dot{q}_m^A J_{0nm}^{RA}\Big\} \sin\psi + \Big\{-\frac{1}{2}\theta_0 \mu^2 C_{0n}^R + \Big(B_1 \mu - \frac{1}{2}\theta_1 \mu^2\Big) C_{1n}^R\Big\} \cos 2\psi + \Big\{-\mu A_1 C_{1n}^R - \frac{1}{2}\mu^2 \sum_m q_m^R K_{0nm}^R - \frac{1}{2}\mu^2 a_0 C_{0n}^R\Big\} \sin 2\psi \Big] - \bar{g}_n^R \sigma_n^R(0) - \bar{a}_n^R \lambda_n^R(0) \tag{40}$$

where

$$\gamma_n^A = \frac{\rho a C R}{m_0 M_n^A}, \gamma_n^R = \frac{\rho a C R}{m_0 M_n^R}, \bar{g}_n^R = \frac{g}{R\Omega^2 M_n^R}, \bar{a}_n^R = \frac{a_0}{M_n^R} \tag{41}$$

$$\theta = \theta_0 + \theta_1 x - A_1 \cos\psi - B_1 \sin\psi$$

is the blade pitch angle, and λ is the inflow ratio. Definitions of other constants are listed in Table 1.

Some interesting facts can be observed in the above equations. First, the cyclic forces vibrate the cyclic modes and the collective forces vibrate the collective modes. Thus the collective pitch oscillates mainly q_n^R, and the cyclic pitch excites mainly q_n^A.

Second, there are intermodal couplings. The cyclic nth mode affects not only the cyclic mth mode, but also the collective modes. Collective modes also affect the cyclic modes. Thus, it is clear that the Blankenship method for calculating the rotor load distribution by simply superposing each sinusoidal result requires careful attention to these couplings.

Third, the nondimensionalized damping coefficients for each elastic mode can be represented by

$$\tfrac{1}{2}\gamma_n^i J_{1nn}^i \qquad (i = A \text{ or } R)$$

For the nonelastic seesaw rotor, the damping coefficient is

$$\gamma/16, \qquad \gamma = \rho a C R^4 / I \qquad \text{(Lock Number)}$$

Since γ_1^A is equal to γ and J_{111}^A is $\frac{1}{8}$, the damping coefficient of the cylic first term is exactly equal to that of the nonelastic

Table 1 Definition of mode constants

No.	Constant	Articulated mode		Rigid mode
1	$M_n^A,\ M_n^R$	$\int_0^1 \bar{m}\phi_n^{A^2}\,dx$		$\int_0^1 \bar{m}\phi_n^{R^2}\,dx$
2	$C_{0n}^A,\ C_{0n}^R$	$\int_0^1 \phi_n^A dx$		$\int_0^1 \phi_n^R dx$
3	$C_{1n}^A,\ C_{1n}^R$	$\int_0^1 x\phi_n^A dx$		$\int_0^1 x\phi_n^R dx$
4	$C_{2n}^A,\ C_{2n}^R$	$\int_0^1 x^2\phi_n^A dx$		$\int_0^1 x^2\phi_n^R dx$
5	C_{3n}^R			$\int_0^1 x^3\phi_n^R dx$
6	J_{0nm}^{AR}		$\int_0^1 \phi_n^A\phi_m^R dx$	
7	J_{0nm}^{RA}		$\int_0^1 \phi_n^R\phi_m^A dx = J_{0mn}^{AR}$	
8	$J_{1nm}^A,\ J_{1nm}^R$	$\int_0^1 x\phi_n^A\phi_m^A dx$		$\int_0^1 x\phi_n^R\phi_m^R dx$
9	$K_{0nm}^A,\ K_{0nm}^R$	$\int_0^1 \phi_n^A \frac{d\phi_m^A}{dx} dx$		$\int_0^1 \phi_n^R \frac{d\phi_m^R}{dx} dx$
10	K_{1nm}^{AR}		$\int_0^1 x\phi_n^A \frac{d\phi_m^R}{dx} dx$	
11	K_{1nm}^{RA}		$\int_0^1 x\phi_n^R \frac{d\phi_m^A}{dx} dx$	
12	$\lambda_n^R(x)$			$\int_x^1 \bar{m}\eta\phi_n^R d\eta$
13	$\sigma_n^R(x)$			$\int_x^1 \bar{m}\phi_n^R d\eta$

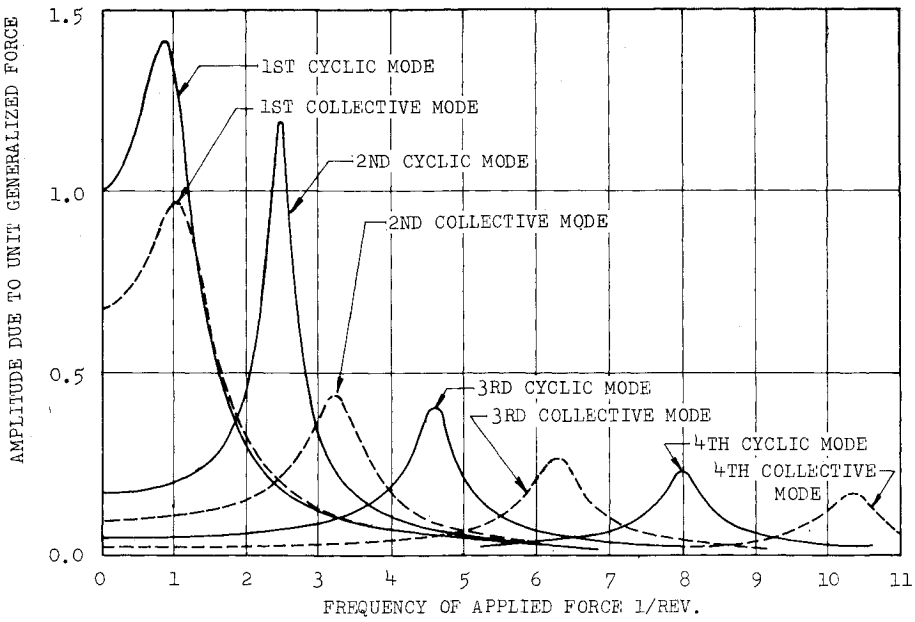

Fig. 3 Resonance curve of elastic modes (UH-1B main rotor).

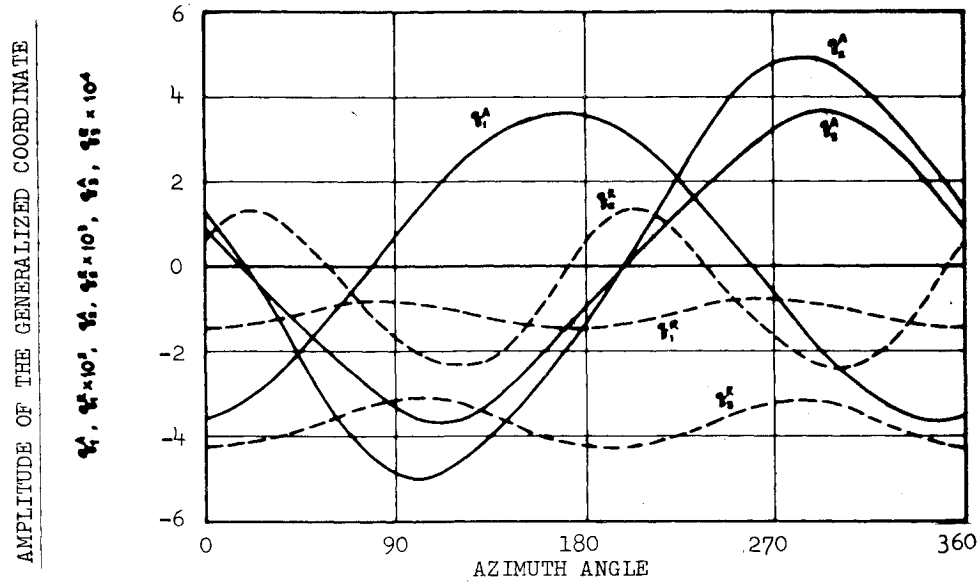

Fig. 4 Sample time history of each elastic mode (UH-1B, 95 kt).

rotor. From the above considerations, γ_n should be regarded as the "generalized Lock Number." It may be understood that the inertia force acting on a nonelastic seesaw rotor is represented by the form of the moment of inertia, I, while it is in proportion to the elastic deflection in the elastic rotor. This is why the generalized Lock Number takes the form of Eq. (41).

Damping coefficients for each elastic mode in the hovering state are given by

$$\zeta_n^i = \frac{\gamma_n^i J_{inn}^i}{4p_n^i} \qquad (i=A \text{ or } R) \qquad (42)$$

Sample Calculations

The mode shapes of the UH-1B helicopter's main rotor are presented in Fig. 2. The blade was devided into 50 sections, and Myklestad's method of vibration analysis was applied. The calculated natural frequencies of the nonrotating blade are within 4% of the experimental values up to the 3rd mode.

The "generalized Lock Number" and the damping coefficients are tabulated in Table 2. Using this table, a resonance curve is calculated and plotted in Fig. 3. In the design of a blade, careful attention should be paid to avoid any resonance. Usually this procedure has been done by using the

Table 2 Generalized Lock Number and damping coefficients[a] (UH-1B main rotor)

Modal order	Cyclic mode			Collective mode		
	γ_n^A	p_n^A	ζ_n^R	γ_n^R	p_n^R	ζ_n^R
1	6.601	1.00	0.381	9.158	1.21	0.379
2	9.214	2.46	0.069_2	11.451	3.24	0.109
3	8.857	4.58	0.058_7	8.570	6.29	0.047_3
4	7.849	7.96	0.034_7	6.961	10.31	0.026_1
5	7.094	12.64	0.022_0	6.061	15.14	0.016_5

[a] γ_n^i = generalized Lock Number; p_n^i = frequency ratio; ζ_n^i = nondimensionalized damping coefficient; $i=A$ or R.

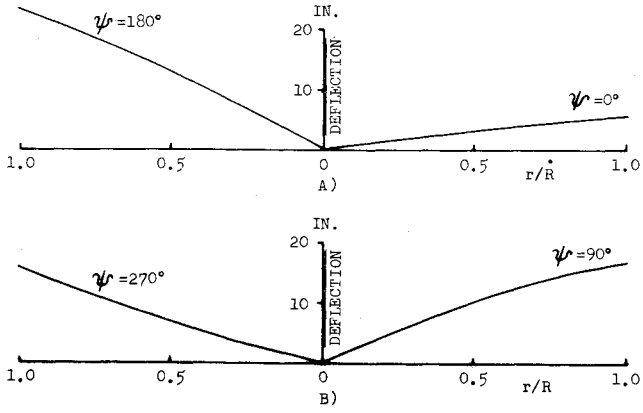

Fig. 5 Illustration of deformed shapes (UH-1B, 95 kt).

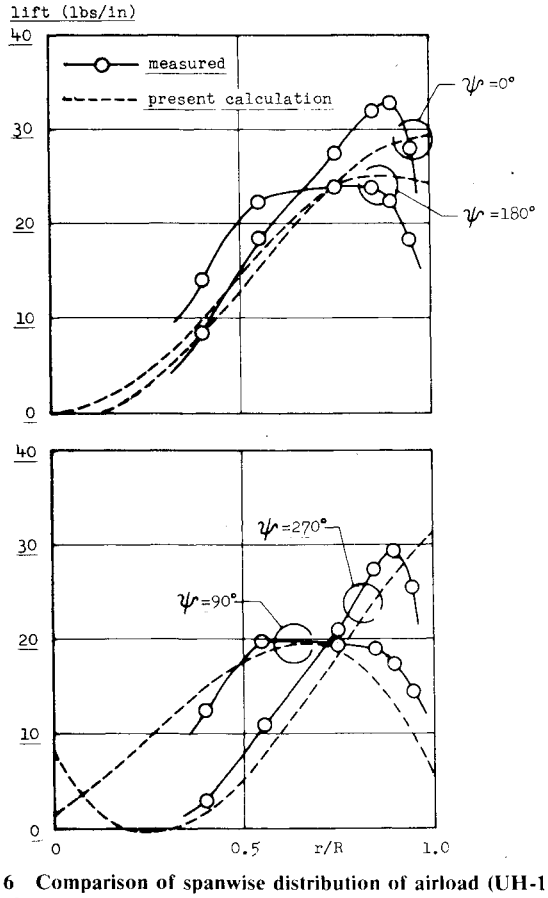

Fig. 6 Comparison of spanwise distribution of airload (UH-1A, 88 kt, 6034 lb, 314 rpm).

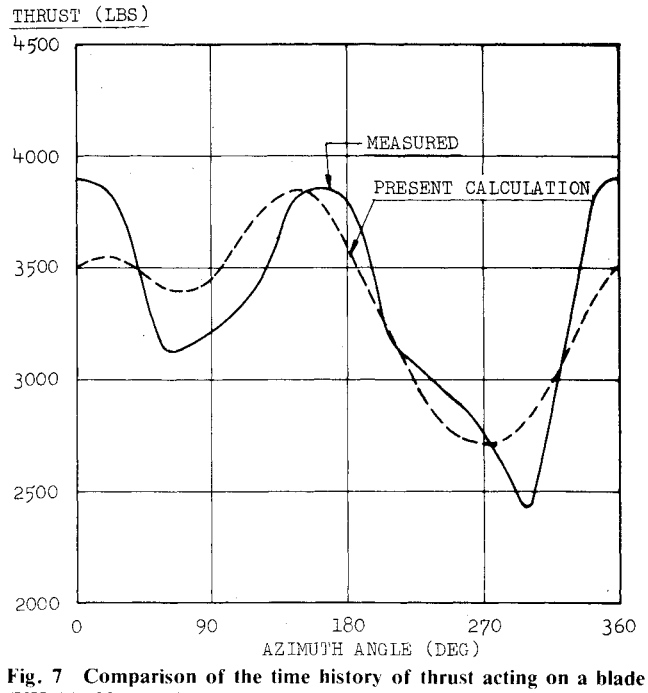

Fig. 7 Comparison of the time history of thrust acting on a blade (UH-1A, 88 kt, 6034 lb, 314 rpm).

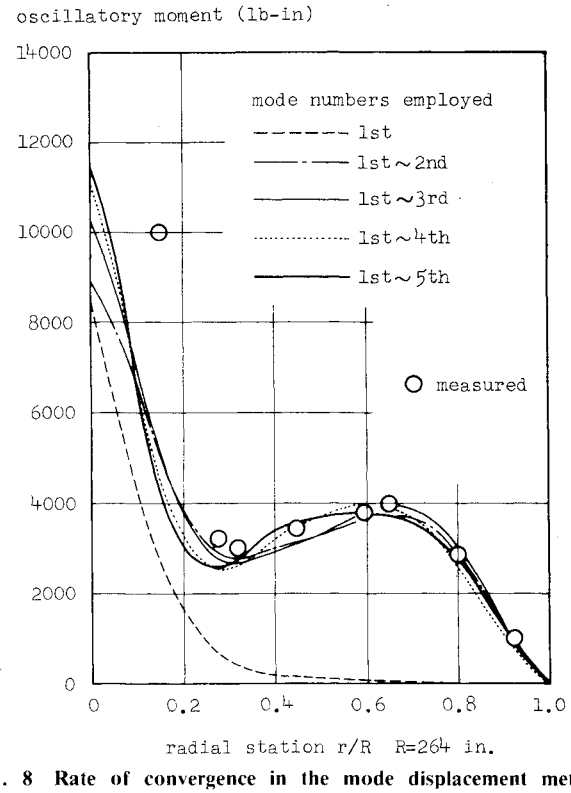

Fig. 8 Rate of convergence in the mode displacement method (MDM) (UH-1A, 88 kt).

so-called $\omega \sim \Omega$ graph (abscissa = shaft angular velocity Ω; orinate = natural frequency of the blade ω). But because this graph does not include the damping effect, it is difficult for the designer of the blade to decide the frequency margin from any one of resonance frequencies. However, if Fig. 3 is used, the decision can be made more easily since Fig. 3 takes into account the damping effect.

Sample time history of the generalized coordinates q_n are presented in Fig. 4. Usually q_n become smaller by one order as the mode number increases by one. From this figure, we can understand that the rotor tilts backward because the tip path plane is almost completely determined by the cyclic first mode q_1^A.

Calculated rotor deflection curves are shown in Fig. 5, in which a) represents the deflection shape viewed from port side and b) from the rear. It is seen clearly that the rotor is flapped back as discussed previously. The preconing angle is almost too large for this thrust condition because the blade is bent such that the upper surface is nearly in tension.

Now, compare the results from the analytical equations with the UH-1A data;[6] this establishes the validity of the analysis. Figure 6 compares the calculated airload with the measured values. The tip loss effect does not appear in the calculated value because the calculation was performed by the two-dimensional strip theory. This is why the calculated value is a little smaller than that measured near the mid span. Figure 7 represents the thrust acting on a blade which is obtained by integrating the airload distribution of Fig. 6. It is rather

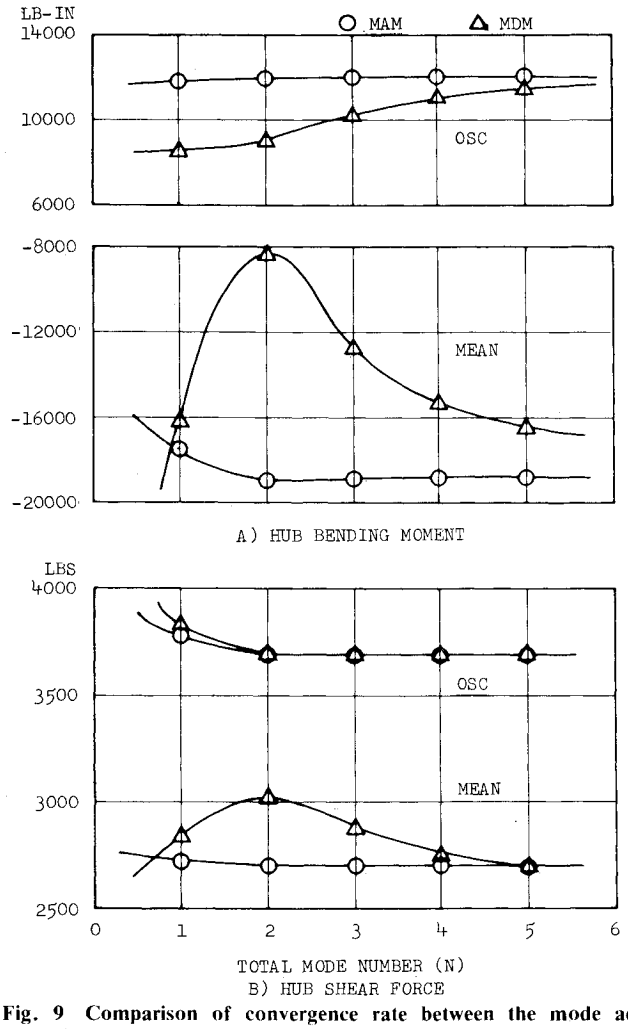

Fig. 9 Comparison of convergence rate between the mode acceleration method (MAM) and the mode displacement method (MDM) (UH-1A, 88 kt).

surprising that the theoretical and the measured curves are correlated well, in spite of the many assumptions made in the theory.

Oscillatory bending moment distribution is presented in Fig. 8. Calculations have been performed using the MDM and varying the total mode number. This figure shows that up to the 5th or still higher modes are required in the MDM for the calculation of a seesaw rotor load distribution. The difference of the convergence rate between the MAM and the MDM is illustrated in Fig. 9 by taking an example of the hub bending moment and shear force. Figure 9 demonstrates clearly that is sufficient to take only the first two modes in the MAM, whereas the MDM bending moment has not yet converged even when five modes are employed. Taking still higher modes is not desirable because the azimuthal step in the calculation of q_n must be smaller (say, 5° or less) as high modes have high natural frequencies.

The time history of the bending moments at the radial station of 60% are presented in Fig. 10. Correlations are relatively good except for the high-frequency loads that appear in the measured data. Lack of high-frequency loads is due to the theoretical assumptions made in the calculation of the airload. These differences will become smaller at high speed if numerical integration that takes account of the nonlinear effects is used with Eqs. (15) and (16). Furthermore the low-speed region can be improved by the variable downwash theory.

Calculated and measured bending moment distribution is presented in Fig. 11. Except at the sta. 40-in. data point, where the measured oscillatory moment is approximately

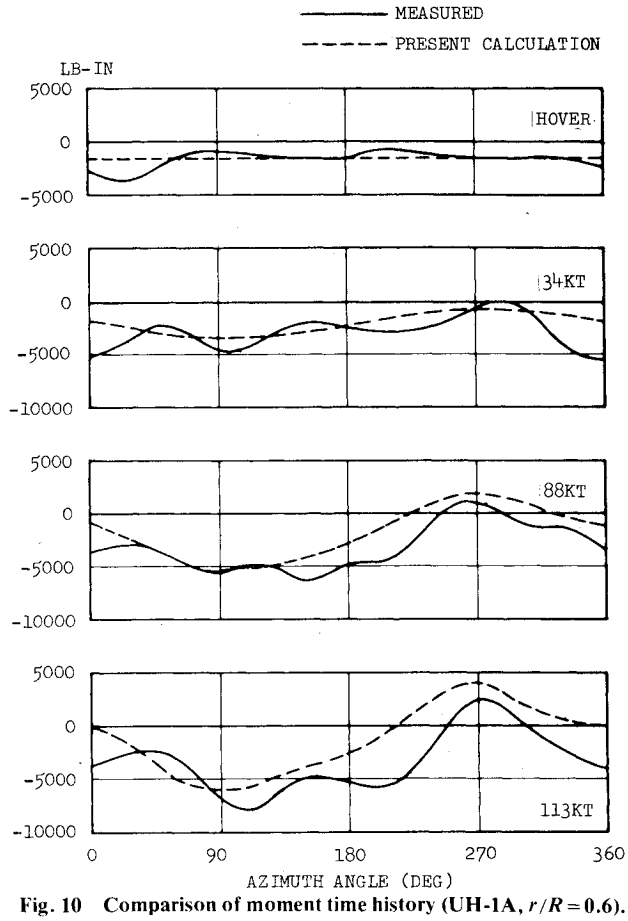

Fig. 10 Comparison of moment time history (UH-1A, $r/R = 0.6$).

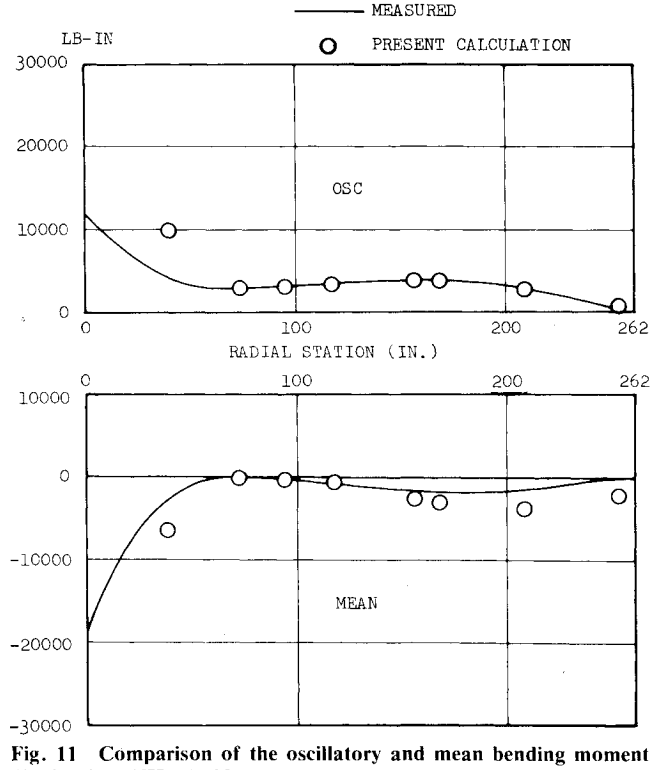

Fig. 11 Comparison of the oscillatory and mean bending moment distribution (UH-1A, 88 kt).

double that of calculated, correlations are satisfactory. Since the difference between the measured and calculated oscillatory moment at the sta. 40 in. is exceptionally large, the same comparison was made for a UH-1B main rotor in Fig. 12. Good agreement exists over the entire rotor. Therefore, it

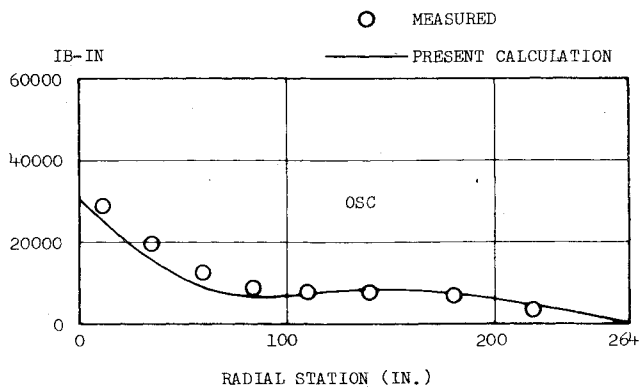

Fig. 12 Comparison of oscillatory bending moment of the UH-1B (113 kt, 6737 lb, 324 rpm).

is suggested that the measured UH-1A sta. 40-in. moment may be in error, but it is impossible to make a more detailed study because of the limited data.

Now, consider the effect of the preconing angle on the mean bending moment distribution. In the design of a seesaw rotor, the mean bending moment distribution is controlled by careful determination of the preconing angle. It would be helpful during the design process if the change of the mean bending moment distribution due to a unit change of the preconing angle were known a priori. Equation (40) can be used for this purpose. Neglecting all terms except the preconing angle, it reduces to

$$p_n^{R^2} q_n^R = -\bar{a}_n^R \lambda_n^R(0) = -\frac{\lambda_n^R(0)}{M_n^R} a_0 \tag{43}$$

Differentiating this equation by a_0 yields

$$\frac{\partial q_n^R}{\partial a_0} = -\frac{1}{p_n^{R^2}} \frac{\lambda_n^R(0)}{M_n^R} \tag{44}$$

From Eqs. (33)-(35) we can write

$$\frac{\partial M}{\partial a_0} = -m_0 R^3 \Omega^2 \left\{ \sum_n \frac{\partial q_n^R}{\partial a_0} (\lambda_n^R - \phi_n^R \tau) + (k - x\tau) \right\} \tag{45}$$

Combining Eqs. (44) and (45) yields

$$\frac{\partial M}{\partial a_0} = m_0 R^3 \Omega^2 \left\{ \sum_n \frac{1}{p_n^{R^2}} \frac{\lambda_n^R(0)}{M_n^R} (\lambda_n^R - \phi_n^R \tau) + (x\tau - k) \right\} \tag{46}$$

A sample calculation has been performed using this equation for the UH-1A rotor. The following value is obtained for the hub moment taking account up to the 3rd modes.

$$\left(\frac{\partial M}{\partial a_0}\right)_{x=o} = -52{,}900 \text{ lb-in./deg} \tag{47}$$

This value is also useful for the determination of the tolerance for the preconing angle. The same calculations can be performed for the determination of the moment or shear force increments due to the g maneuver, wash-out change, and the collective pitch change.

As the last example, Fig. 13 presents the effect of elastic deformation in the calculation of the airload on the moment distribution. Simplified analysis which ignores the effect of the elastic deformation on the airload has been used frequently in the practical design stage. Few reports have been published stating accuracy without elastic deformation. From

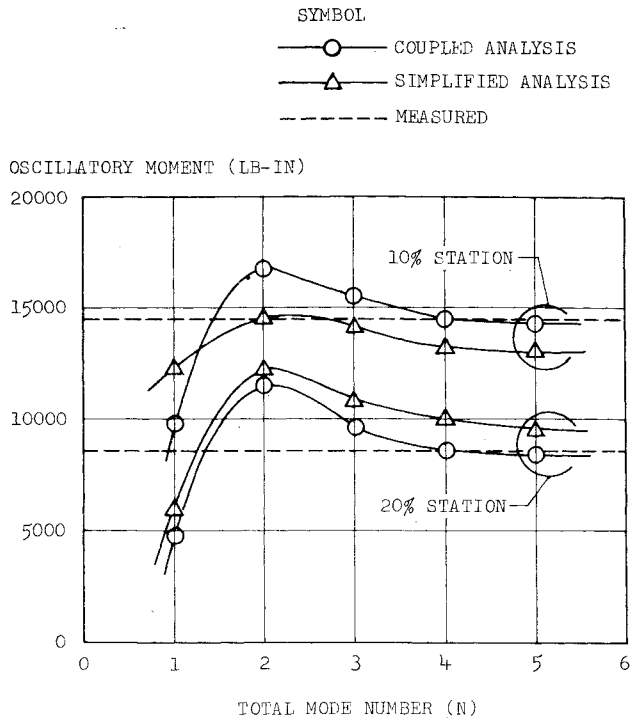

Fig. 13 Study of accuracy of the simplified analysis (elastic deformation is neglected in the calculation of airload UH-1B, 100 kt).

Fig. 13, it is apparent that a 10% error in the oscillatory moment may occur.

Conclusions

The collective modes and the cyclic modes couple to each other if the equation of motion of an elastic seesaw rotor is described by the modal method. A technique has been developed to separate this coupling with the result that the derived equation is similar to that of the rigid or the articulated rotor. This equation is an extension of Gessow's method for elastic motion and, at the same time, includes Blankenship's load calculation method for a seesaw rotor in a more refined fashion.

Making some assumptions and applying the classical representation for airloads, an analytic representation of the equation is obtained. A study was conducted to establish the validity of this equation. The usefulness of the equation was demonstrated for the dynamics of an elastic seesaw rotor. Calculations were performed using this equation and the following results are clear.

1) The "generalized Lock Number" for the each elastic mode is

$$\gamma_n = \frac{\rho a c R^2}{\int_0^R m \phi_n^2 dr}$$

2) The damping coefficient for the each elastic mode in the hovering state is

$$\zeta_n = \frac{\gamma_n \int_0^1 \phi_n^2 x dx}{4\omega_n/\Omega}$$

3) A resonance curve for the elastic oscillation is written by taking account of the damping effect represented in the item 2; using the resonance curve it is easy to predict how each elastic mode will respond to any oscillating force.

4) $2n$/rev harmonics of the force vibrate the collective modes and $2n+1$/rev harmonics of the force vibrate the cyclic modes; thus the cyclic pitch affects mainly the cyclic modes, whereas the collective pitch, the blade twist, and the preconing angle are affected mainly by the collective modes.

5) The cyclic modes and the collective modes couple aerodynamically.

6) Up to the 5th or still higher modes are required in the calculation of rotor loads in the mode displacement method (MDM), but only 2 or 3 modes are necessary for convergence if the mode acceleration method (MAM) is employed.

7) The effect of neglecting the elastic deformation in the airload calculation leads to a 10% error in the oscillatory moment.

8) Additional moment change over the blade caused by the change of preconing angle can be estimated without solving the total equation of motion; likewise, the moment increment due to g maneuver or the static deflection of the rotor at rest are easily calculated.

References

[1]Gessow, A. and Crim, A.D., "A Method for Studying the Transient Blade-Flapping Behavior of Lifting Rotors at Extreme Operating Conditions," NACA TN 3366, Nov. 1954.

[2]Blankenship, B.L. and Harvay, K.W., "A Digital Analysis for Helicopter Performance and Rotor Blade Bending Moments," *Journal of the American Helicopter Society*, Vol. 7, Oct. 1962, pp. 55-68.

[3]Bisplinghoff, R.L., Holt, A., and Halfman, R.L., *Aeroelasticity*, Addison-Wesley, Reading Mass., 1955, pp. 632-650.

[4]Shupe, N.K., "A Study of the Dynamic Motion of Hingeless Rotored Helicopters,"United States Army Electronics Command, Fort Monmouth, N.J., ECOM-3323, Aug. 1970.

[5]Bramwell, A.R.S., "A Method for Calculating the Stability and Control Derivatives of Helicopters with Hingeless Rotor," The City Univ., London, RM Aero 69/4 June, 1970.

[6]Bell Helicopter Company, "Measurement of Dynamic Air Loads on a Full-Scale Semirigid Rotor," U.S. Army Transportation Research Command, Fort Eustis, Va., TCREC Technical Report 62-42, AD 297940, Dec. 1962.